2005

Wintertime boundary-layer structure and air-sea interaction over the Japan/East Sea

Khelif, Djamal

þÿ D e e p - S e a R e s e a r c h I I , V o l . 5 2 , (2 0 0 5) , p p . 1 5 2 5 1 5 4 6
http://hdl.handle.net/10945/46135

ELSEVIER

Deep-Sea Research II 52 (2005) 1525–1546

DEEP-SEA RESEARCH
PART II

www.elsevier.com/locate/dsr2

Wintertime boundary-layer structure and air–sea interaction over the Japan/East Sea

Djamal Khelif[a,*], Carl A. Friehe[a], Haflidi Jonsson[b], Qing Wang[b], Konstantinos Rados[c]

[a]*Department of Mechanical and Aerospace Engineering, University of California, Irvine, CA 92697-3975, USA*
[b]*Department of Meteorology, Naval Postgraduate School, Code MR/Qg, 589 Dyer Road, Monterey, CA 93943-5114, USA*
[c]*School of Mechanical and Offshore Engineering, The Robert Gordon University, Schoolhill, Aberdeen AB10 1FR, Scotland*

Received 12 July 2002; received in revised form 26 July 2003; accepted 8 April 2004
Available online 3 August 2005

Abstract

The wintertime meteorology over the Japan/East Sea (JES) is characterized by episodic strong northwesterly winds known as "cold-air outbreaks" resulting from the incursion of dry and cold air masses from the Eurasian continent. These were found by previous studies (mostly based on indirect methods) to greatly enhance the air–sea interaction and, in particular an area about 150 km in diameter off Vladivostok was identified as the Flux Center. Aircraft in situ measurements of turbulent fluxes and mean meteorological variables were made during the winter 2000. The existence and location of the Flux Center were confirmed although the turbulent sensible and latent-heat fluxes were not as high as previously found due to the air temperature being several degrees warmer. However, the stress was found to be significantly larger as a result of higher wind speeds. The internal boundary layer was found to grow linearly with the square root of offshore fetch, with a growth rate of $2.49\,m^{1/2}$ for an intense cold-air outbreak and $2.06\,m^{1/2}$ for a moderate one. A persistent initial decrease in the inversion height was observed at 41.86°N, 132.6°E and may be attributable to the fanning out of the jet flow out of the Vladivostok gap as it expands onto the open ocean. The radiometric skin sea-surface temperature in the Flux Center exhibited large variability in the 0–4 °C range and was positively correlated with the total turbulent (latent + sensible) heat loss. Meteorological variables and surface fluxes results from Naval Research Laboratory Coupled Ocean/Atmosphere Mesoscale Prediction System (COAMPS) model compared reasonably, while the predictions of the internal boundary layer height were markedly lower than the observations.

1. Introduction

The interaction of the atmosphere and ocean over the Japan/East Sea (hereafter the JES) during

*Corresponding author.
E-mail address: dkhelif@uci.edu (D. Khelif).

0967-0645/$ - see front matter © 2005 Elsevier Ltd. All rights reserved.
doi:10.1016/j.dsr2.2004.04.005

winter is characterized by periods of strong, cold and dry air flow off Siberia. Wintertime northwest winds across the JES can be quite large with the establishment of the Siberian High and on the back side of cyclones (Manabe, 1957). (We use the meteorological convention for wind direction—north winds are from the north.) If the wind-stress input to the ocean and heat and water vapor (buoyancy) losses from the ocean are large enough for a long enough time, over-turning of the water column may occur. Similar situations are found in the Gulf of Lions in the Mediterranean Sea during Mistral winds (MEDOC Group, 1970) and in other enclosed or semi-enclosed ocean basins like the JES. The atmospheric situation for the JES is further complicated by local topographic effects due to channeling of the off-shore winds through the Vladivostok gap and orographic lifting as the flow approaches Honshu Island of Japan. Recently, Kawamura and Wu (1998) combined satellite scatterometer winds, surface analyses from the European Center for Medium-range Weather Forecasting (ECMWF), and Japan Meteorological Agency (JMA) sea-surface temperature data to show that in winter there is an area about 150 km in diameter off Vladivostok (41.25N, 132.5E) of extremely high air–sea interaction which they termed the Flux Center. They defined it for January 1997 as the area bounded by contours of monthly means of 0.275 Pa for stress, 170 $W m^{-2}$ for sensible-heat flux and 130 $W m^{-2}$ for latent-heat flux. The maximum contours in the Flux Center were then 0.325 Pa, 210 $W m^{-2}$ and 400 $W m^{-2}$ for stress, sensible-heat flux and total (sensible + latent) turbulent heat flux, respectively.

As the cold, dry air flows over the relatively warm ocean, an internal marine atmospheric boundary layer is expected to develop with fetch offshore. The persistent sea-surface temperature front in the JES at approximately 40°N may further modify the internal boundary layer. Detailed measurements of the air–sea fluxes and boundary-layer structure are not common in wintertime cold air outbreak (hereafter CAO) situations. Such measurements provide insight into the meteorology, oceanic forcing and air–sea interaction. They also provide good tests for mesoscale models. The purpose of this paper is to present results of the research aircraft portion of the winter-time JES experiment in January–February 2000 and comparison to a mesoscale model, COAMPS (Hodur, 1997).

2. Experiment

A research aircraft was used for the measurement of air–sea fluxes and meteorological parameters. The aircraft was the Twin Otter of the US Naval Postgraduate School's Center for Interdisciplinary Remotely-Piloted Aircraft Studies (CIRPAS). The instrumentation was similar to that used on other research aircraft (Khelif et al., 1999) and is listed in Table 1. A photograph of the aircraft showing the placement of the major instruments is presented in Fig. 1. For redundancy, two data systems were used. One recorded the data at 40 Hz and the other at 10 Hz, and data from each system were processed to yield meteorological data at 1 Hz and turbulence data at either 40 or 10 Hz.

Flights were flown from Misawa NAF in Japan out to the Flux Center off Vladivostok, Russia. Three basic flight patterns were performed: flux mapping (FM) at 30 m nominal altitude, flux divergence (FD), both in the vicinity of the Flux Center, and internal boundary-layer (IBL) transects across the JES. Fig. 2 shows typical FM and IBL flight patterns. There were a total of 12 flights: five FM, five IBL and two FD. The Asian Coastal Buffer Zone and other airspace regulations restricted the flights to east of 132°E and south of 42.25°N. Each flight was over 9 h long and, depending on the pattern flown, the on-station time varied between 3.5 and 5 h, which corresponded approximately to mid-morning to late afternoon local time.

The dates and times given are UTC and follow the format yymmdd (e.g. 000218 for February 18, 2000) and hh:mm:ss, respectively.

3. Flux mapping

Grid patterns were flown over the nominal area of the Flux Center under CAO conditions at the

Table 1
CIRPAS Twin Otter JES instrumentation

Parameter	Instrument[a]	Location	Fast/slow[b]
Position	Boeing C-MIGITS II (GPS/INS)	Nose	F
	Trimble TansVector (GPS)	Wings and Fus., top	F
	NovAtel GPS	top Fus.	S
Ground speed vector	Boeing C-MIGITS II (GPS/INS)	Nose	F
	Trimble TansVector (GPS)	Wings and Fus., top	F
Attitude angles	Boeing C-MIGITS II (GPS/INS)	Nose	F
	Trimble TansVector (GPS)	Wings and Fus., top	F
Aircraft altitude	Collins ALT-50 Radar Altimeter	Belly	S
Humidity	AIR-LA-IC Lyman-α Hygrometer (**2**)[c]	Nose and top Cabin	F
	Campbell Sci. Krypton Hygrometer KH2O	Fuselage, back	F
	NOAA/ATDD IRGA Hygrometer	Nose	F
	EdgeTech Dewpointer 137-C3	Nose	S
	Vaisala HMD70Y	Nose	S
Recovery temperature	Rosemount 102E4AL	Nose	F
	UCI-modified Rosemount (**4**)[c]	Nose	F
Airspeed vector			
$\Delta P_\alpha, \Delta P_\beta$ {Differential Attack, Sideslip Pressure}	Rosemount 858AJ 5-hole Probe Setra 239 Transducers	Nose, center	F
	Flush Radome Pressure Ports Setra 239 Transducers	Radome	F
P_{qm} {Dynamic Pressures}	Aero Instrument Pitot Tube Setra 239 Transducer	Fuselage, Starboard	F
	Flush Radome Pressure Port Setra 239 Transducer	Radome	F
	Rosemount 858AJ 5-hole Probe Setra 239 Transducer	Nose, center	F
Static pressure	Flush pressure ports Setra 270 Transducer	Fuselage	F
	Rosemount 858AJ probe Setra 270 Transducer	Nose	F
IR sea-surface temperature	Heiman KT19.85 Radiometer	Belly	S
	Tasco THI-700L	Belly	S
SW $\downarrow$ irradiance (total, partial)	Eppley PSP	Fuselage, top	S
LW $\downarrow$ irradiance	Eppley PIR	Fuselage, top	S
IR sky temperature	Tasco THI-700L	Fuselage, top	S
CO_2 concentration	NOAA/ATDD IRGA	Nose	F

[a]GPS: Global Positioning System, INS: Inertial Navigation System.
[b]Fast-response sensor, S: Slow-response sensor.
[c]Number of identical sensors.

lowest possible altitude of 34–42 m. Time series of potential temperature, water vapor density and vertical, along-wind and cross-wind wind components (θ, ρ_v, w, u_a and u_c, respectively) obtained from the first 10 km of a cross-wind leg flown on 000228 at an altitude of 40 m and approximately

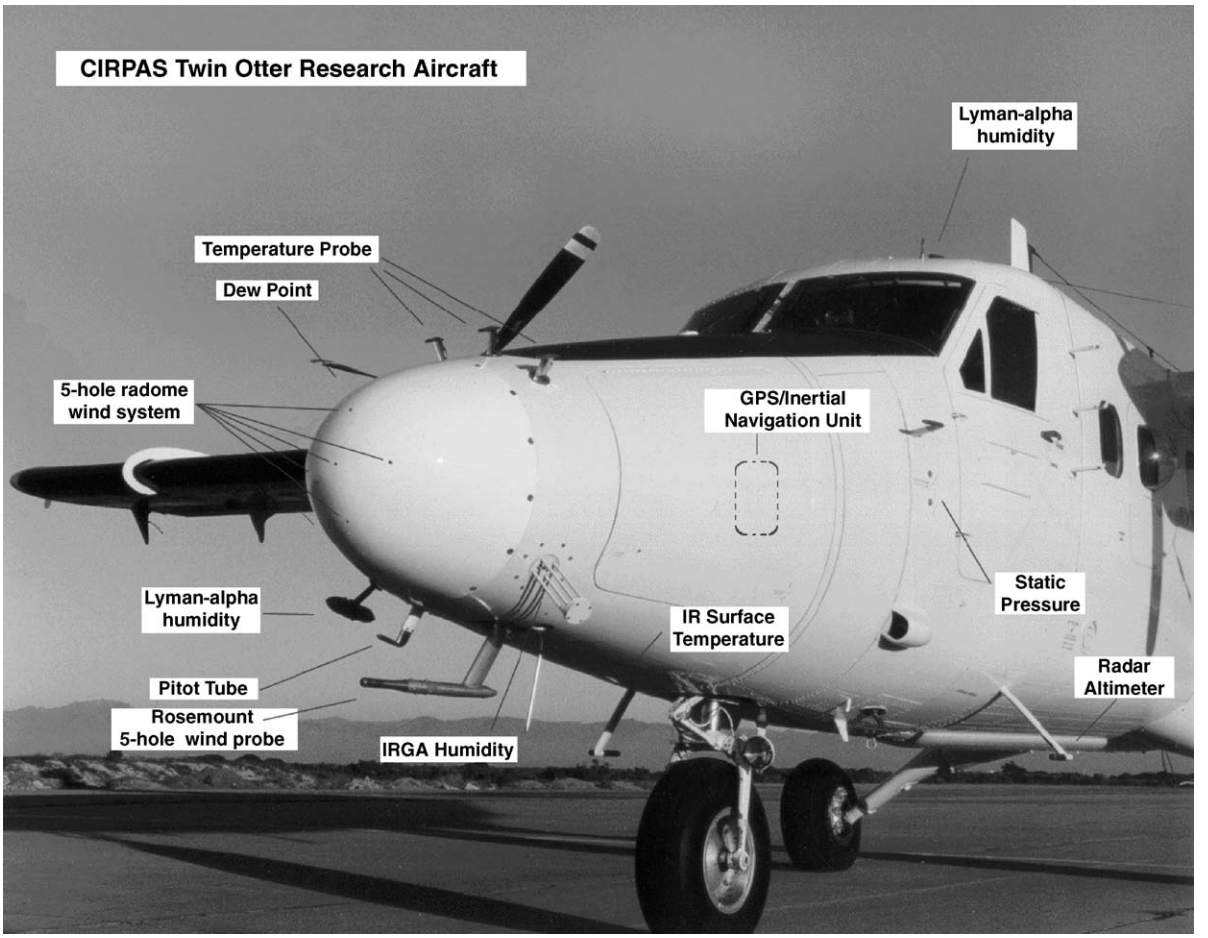

Fig. 1. CIRPAS Twin Otter aircraft with instrumentation for JES. (See Table 1 for more details on the instruments.)

158 km from Vladivostok are shown in Fig. 3. This was a classic cold-air outbreak day with mean surface winds of $19\,\mathrm{m\,s^{-1}}$ and wind gusts up to $26\,\mathrm{m\,s^{-1}}$. The quasi-periodic and well-correlated surges in θ, ρ_v and w are signatures of the flux-carrying eddies of different wavelengths. The larger structures may be associated with the longitudinal (along wind) convective roll vortices prevalent in CAO conditions and similar to those presented in the review of Etling and Brown (1993) and those more recently observed by Hartmann et al. (1997) and Renfrew and Moore (1999). In the latter study, however, no roll signature was observed on the ambient temperature signal.

With the processed high-rate (40-Hz or 10-Hz) data and from the definitions of the Reynolds averaged covariances between the vertical velocity fluctuations and fluctuations of the appropriate quantity, the along-wind-stress, cross-wind-stress, sensible-heat and latent-heat fluxes can be determined as $\tau_a = -\rho\overline{w'u'_a}$, $\tau_c = -\rho\overline{w'u'_c}$, $Q_h = \rho c_p\overline{w'\theta'}$ and $Q_e = L_v\overline{w'\rho'_v}$, respectively, where ρ is the air density, c_p the air specific heat at constant pressure, ρ_v the water vapor density (absolute humidity) and L_v the latent-heat of vaporization, and where the primes indicate fluctuating quantities. The physical properties ρ, c_p and L_v were calculated using the mean values of the

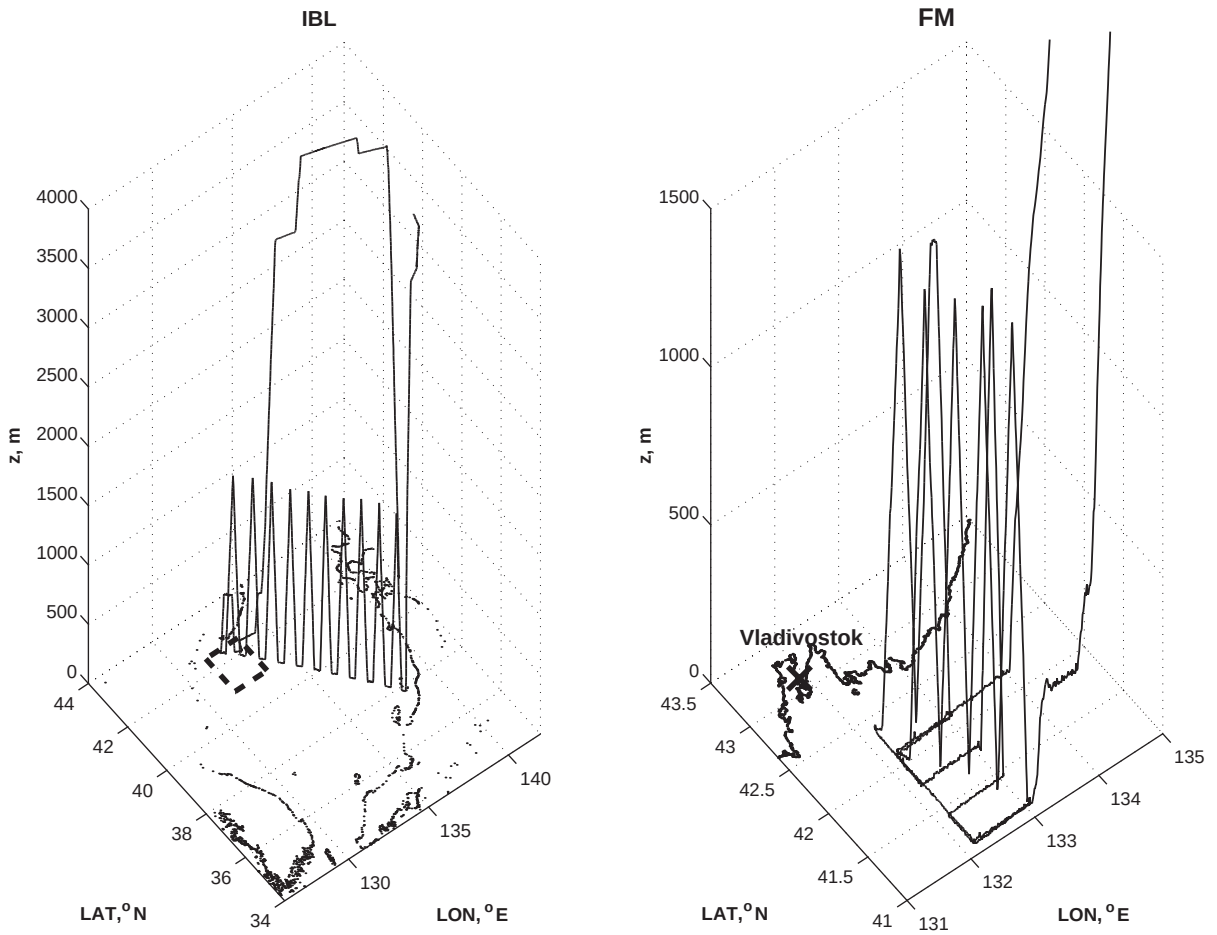

Fig. 2. CIRPAS Twin Otter flight patterns during winter 2000 JES experiment: Internal boundary-layer (IBL) pattern across the JES (left) with the approximate location of the Flux Center (Kawamura and Wu, 1998) indicated by the dashed line and flux mapping (FM) pattern in the Flux Center (right).

meteorological variables on each flux run. The total stress is determined as $\tau = (\tau_a^2 + \tau_c^2)^{1/2}$.

From spectral analysis, the fluxes are also the integrals of the co-spectra between the vertical velocity and the appropriate variable. Sample co-spectra are shown in Fig. 4, along with their cumulative integrals (so-called "ogives"), which provide an indication of convergence towards good flux estimates (Friehe et al., 1991). Flux ogives that do not exhibit smooth convergence to asymptotic values are indications of non-stationary sample time series or insufficient run lengths. The spectral results shown are from the same cross-wind run in Fig. 3 but for the entire 37-km run. The ogives show that most of the flux (80%) is carried by eddies with wavelength between 100 m and 4 km. The peaks in the cospectra at the mid-range wavelengths correspond to the main flux carrying eddies and the one at 2.8 km is believed to be associated with the longitudinal roll vortices. The cospectra from another run flown 1 h later at 93 m on the same track showed a more prominent peak at about 2.9 km around which the sensible and latent-heat ogives increased by 18% and 21%, respectively.

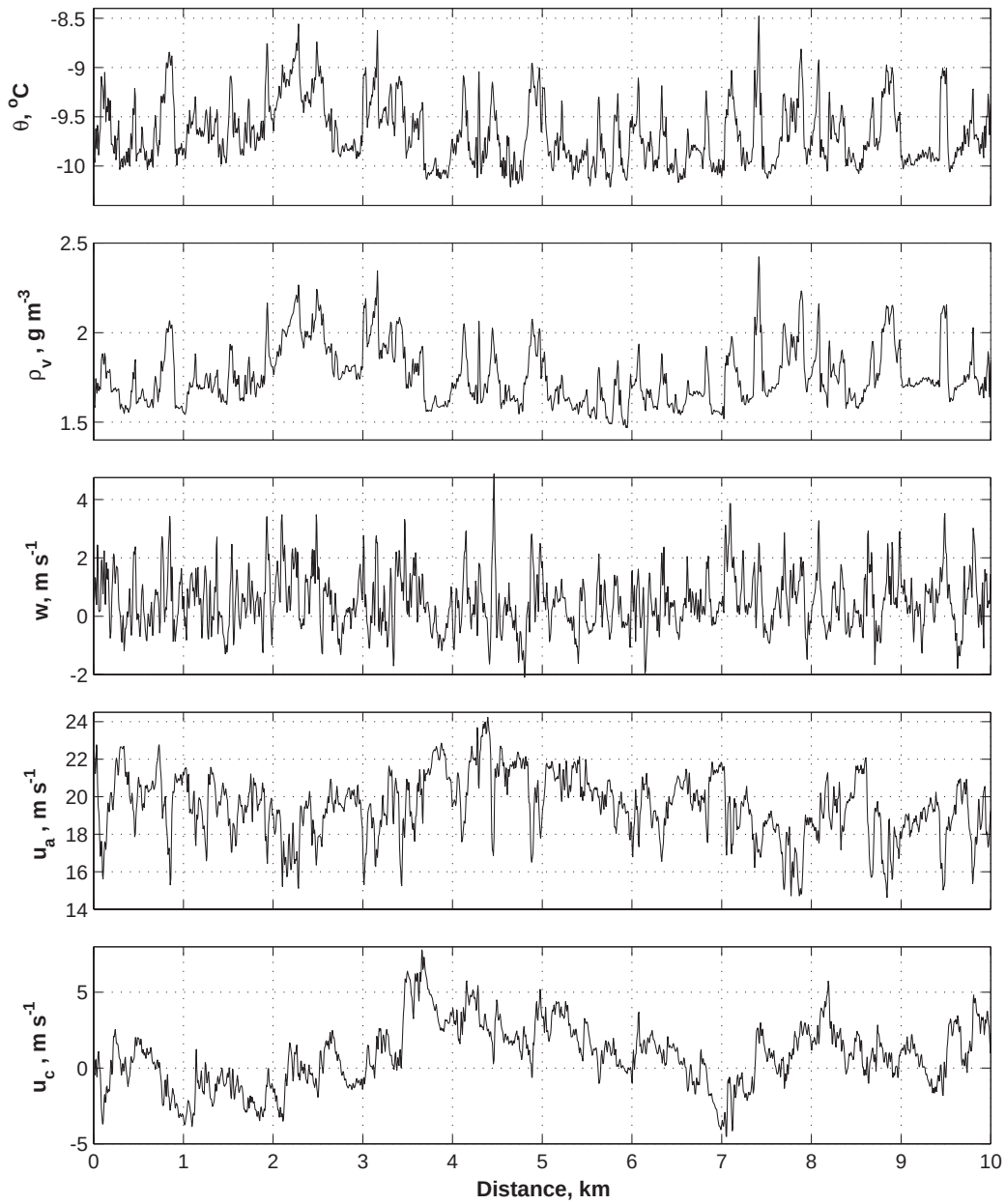

Fig. 3. Time series of, from top to bottom, potential temperature (less 273.15 K), θ; water vapor density, ρ_v; vertical; along-wind; and cross-wind air velocities w, u_a and u_c, respectively. Data are from the first 10 km of a 37-km cross-wind run flown at 40 m above sea level in the Flux Center 158 km off the coast on 000228 at 01:45:56–01:48:38 UTC (1 km corresponds to 15.5 s.) The correlated and quasi-periodic surges in θ, ρ_v and w correspond to flux-carrying eddies of different wavelengths. The larger ones may be signatures of along-wind roll vortices.

These values are comparable to the 26.5% and 20.5% found by Hartmann et al. (1997) and which they attributed to the longitudinal roll vortices.

Maps of the fluxes are shown in Fig. 5 for a moderate CAO on 000201 and Fig. 6 for a stronger CAO on 000209. Within the Flux Center and on the

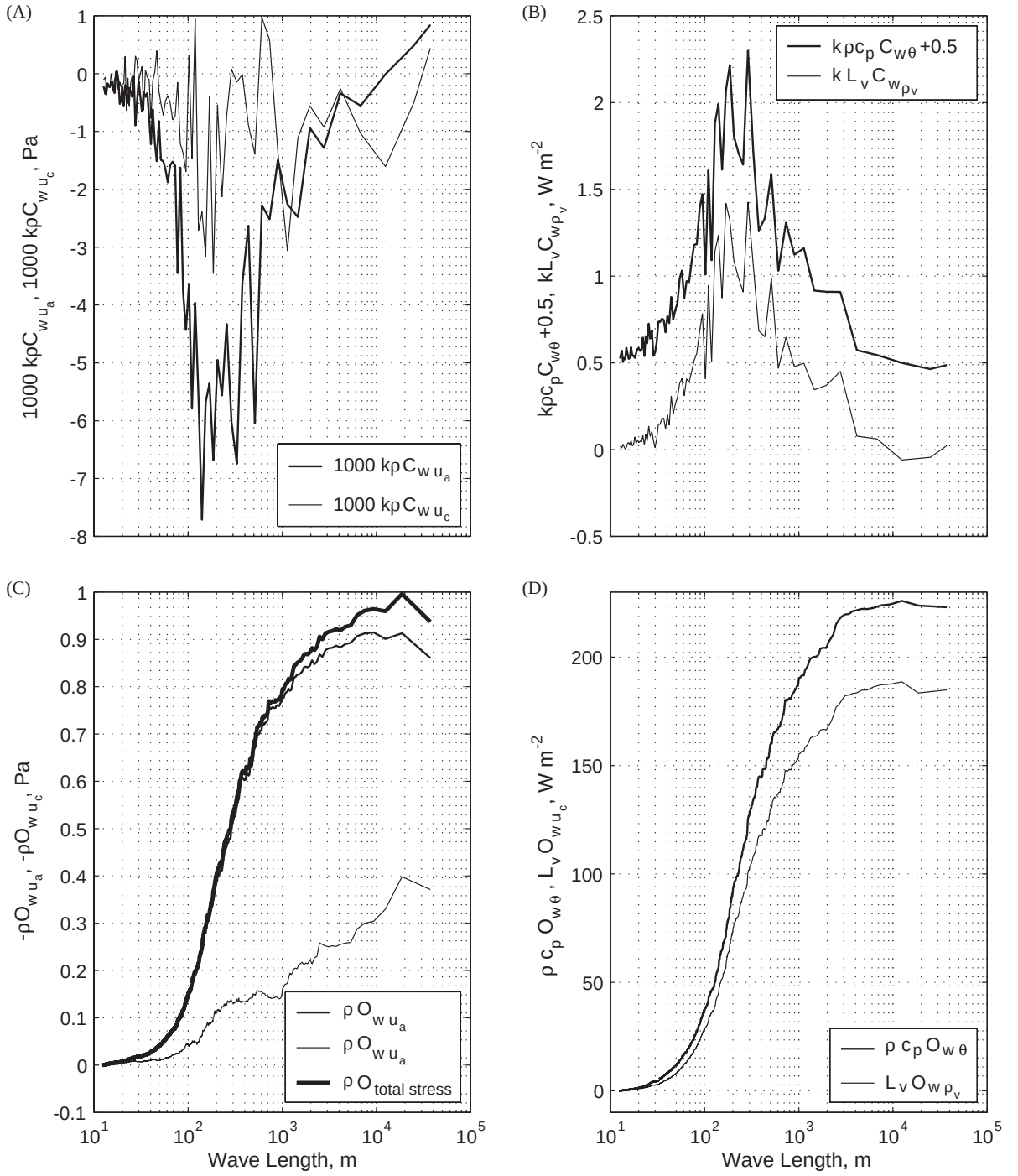

Fig. 4. Cospectra (A) and ogives (C) of cross-wind (thin), along-wind (thick) and total (thicker) momentum fluxes; cospectra (B) and ogives (D) of sensible (thick) and latent (thin) heat fluxes. The ogives are calculated as the cumulative integrals of the cospectra, (e.g., $O_{w\theta}(k) = \int_{\infty}^{k} C_{w\theta}(k)\,dk$ where k is the wave number and $C_{w\theta}$ the cospectrum between the fluctuations of w and those of θ.) Note that $0.5\,\mathrm{W\,m^{-2}}$ has been deliberately added to $k\rho c_p C_{w\theta}$ for clarity.

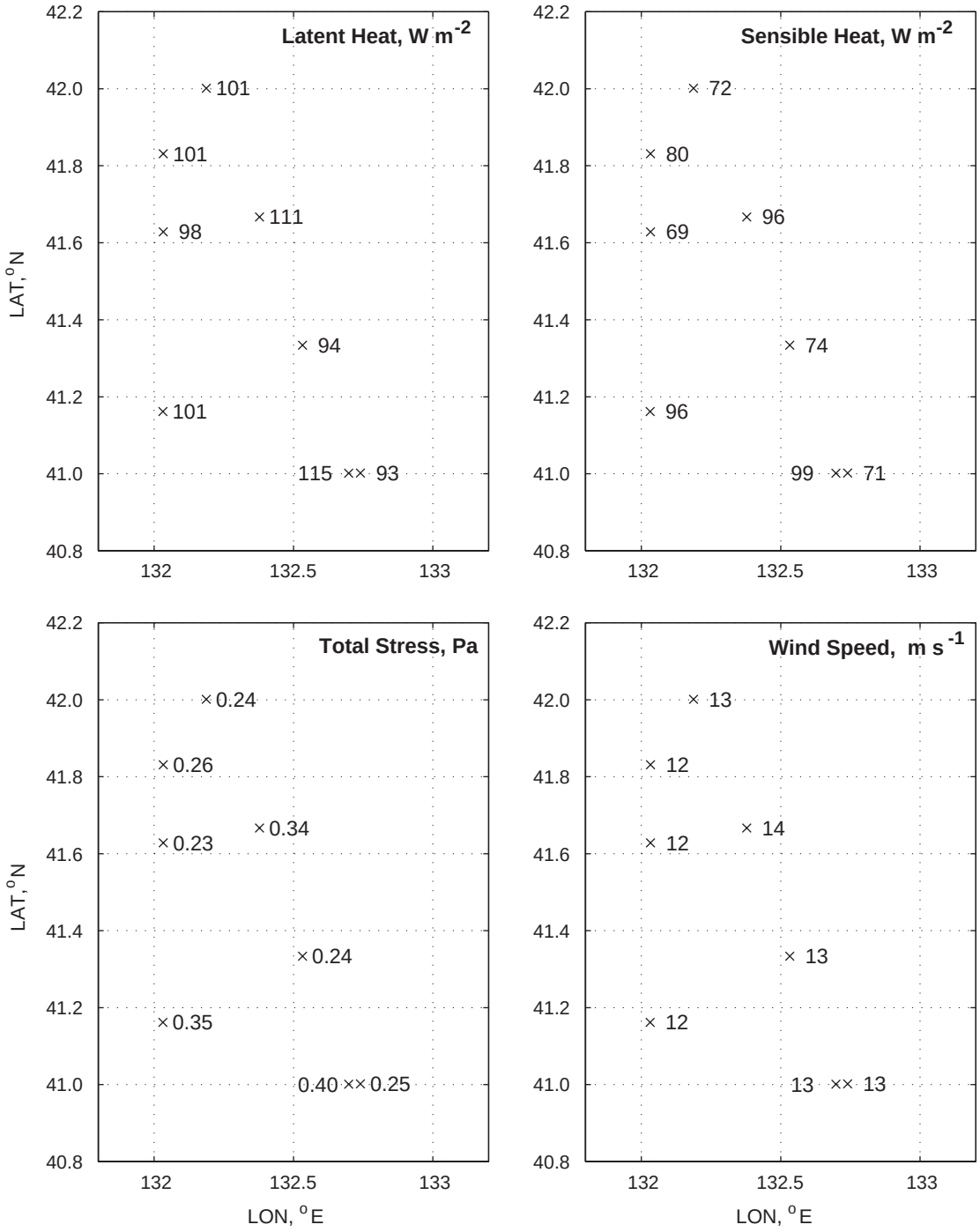

Fig. 5. Spatial variability of turbulent fluxes of latent (top, left), sensible (top, right) heats and total stress (bottom,left) in the Flux Center on 000201 during 00:53:00–03:39:00 UTC. The wind speed (bottom, right) is given as an indication of the cold-air outbreak conditions. The mean wind direction (not shown) was 315°.

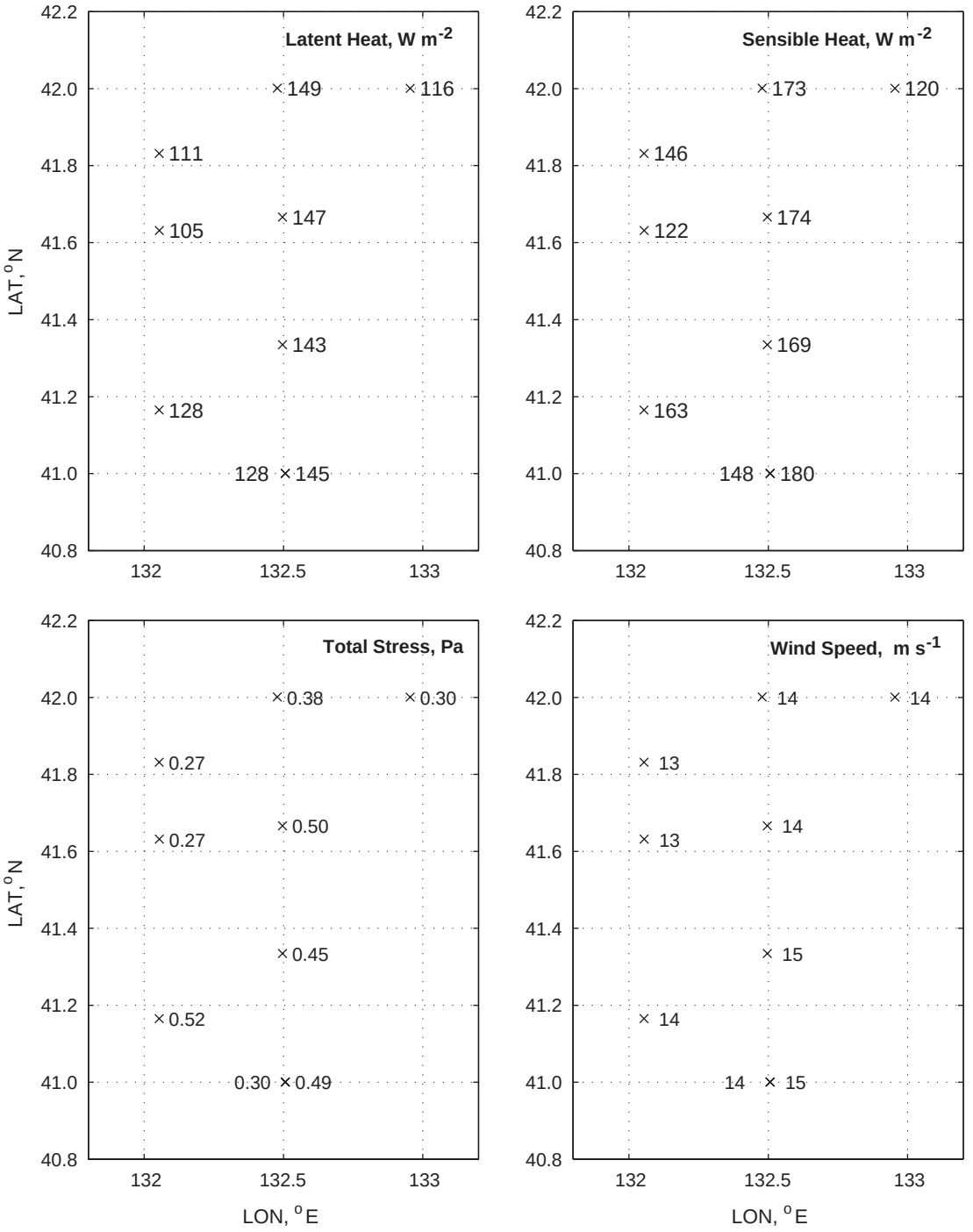

Fig. 6. Spatial variability of turbulent fluxes of latent (top, left), sensible (top, right) heats and total stress (bottom, left) in the Flux Center on 000209 during 01:32:18–05:38:18 UTC. The wind speed (bottom, right) is given as an indication of the cold-air outbreak conditions. The mean wind direction (not shown) was 330°.

same day, the spatial variability of the fluxes and meteorological data were not large and did not display any particular pattern. Results from the three other FM flights confirmed this finding.

Results of previous studies (Khelif et al., 1999; Burns et al., 1999) of numerous side-by-side comparisons of aircraft with similar turbulence instrumentation showed differences of 3.5 ± 15, $0 \pm 2.5\,\mathrm{W\,m^{-2}}$ and $0 \pm 0.015\,\mathrm{Pa}$ in latent, sensible and momentum fluxes, respectively. These differences are representative of the uncertainty associated with the aircraft turbulence measuring system as a whole.

4. Internal boundary layer

IBL patterns were flown starting near Vladivostok and flying along a downwind track determined from initial wind direction at the starting point. Track adjustments were not made to compensate for changes in wind direction. Repeated sequences of up-and-down profiles were flown along the track climbing from 30 m to above the marine inversion and back down to 30 m at average rates of $4.5\,\mathrm{m\,s^{-1}}$. At the base of the profiles, 5-min level runs at 30 m were made to obtain flux estimates as well as mean meteorological surface variables. Typically, 10 pairs of profiles and 10 fluxes were obtained across the JES. Air traffic control limited the profiles to below 1524 m.

The pattern provided measurements of the growth of the IBL with the offshore fetch, F, across the JES as the outbreak air mass slowed, moistened and warmed due to air–sea interaction. Profiles with well-demarked IBL growth are shown in Fig. 7 for 000203. For the sake of clarity, profile data from only four select soundings (S2, S5, S9 and S17) out of the 22 flown along the south-west track are shown. The IBL height, z_i, was determined from the potential temperature jump across the inversion. It increased from about 300 m in the northern part of the JES to roughly over 1100 m at the southern end in response to the abrupt change in surface conditions from land to ocean. It is interesting to note that since the SST also increased across the JES, the temperature difference between the sea-surface and the overlying warming air remained almost constant at $\approx 8-10\,^{\circ}\mathrm{C}$. The SST front in the JES was crossed at about 500 km from the coast (latitude $\approx 39.5^{\circ}\mathrm{N}$), and the sharp increase in z_i there appears to be in response to it.

While the data from Fig. 7 show an expected growth of the IBL with fetch, many profiles nearest the Vladivostok gap showed an initial higher inversion which decreased to a minimum before increasing further across the JES. Such profiles are shown in Fig. 8 for two days. The decrease in the initially higher z_i is thought to be due to the boundary layer fanning out downstream of the gap. This is in qualitative agreement with the stratified flow model results of Scotti (2005). Thereafter, the inversion height increases due to air–sea interaction.

The growth of the IBL with the square root of offshore fetch was predicted by Venkatram (1977) and described in Stull (1988, Chap. 14). As shown in Fig. 9, a strong correlation between z_i and $F^{1/2}$ was found with high coefficient of determination (R-squared) values of 0.97 and 0.99 for 000203 and 000218, respectively. Since the flight tracks from the two flights were almost identical and followed the streamline, and the mean wind direction differed by only 12° between the two days, the offshore fetch was calculated from the point where the extrapolated common track intersected the coast line, which was found to be 42.86N, 131.44E. The least-square linear fit of z_i to $F^{1/2}$ is good for both days. Because of the decrease in z_i discussed above, the first data point from 000218 and the first two data points from 000203 were excluded from the fits. The growth rate of $2.06\,\mathrm{m^{1/2}}$ obtained for 000203 is somewhat close to the $1.91\,\mathrm{m^{1/2}}$ found near shore by Hsu (1986). The higher growth rate of $2.49\,\mathrm{m^{1/2}}$ found for 000218 may be the result of the more intense CAO conditions prevailing on that day.

5. Surface fluxes and variability

5.1. Variability in the Flux Center

To gain some insight on the variability throughout the one-month deployment period, all available

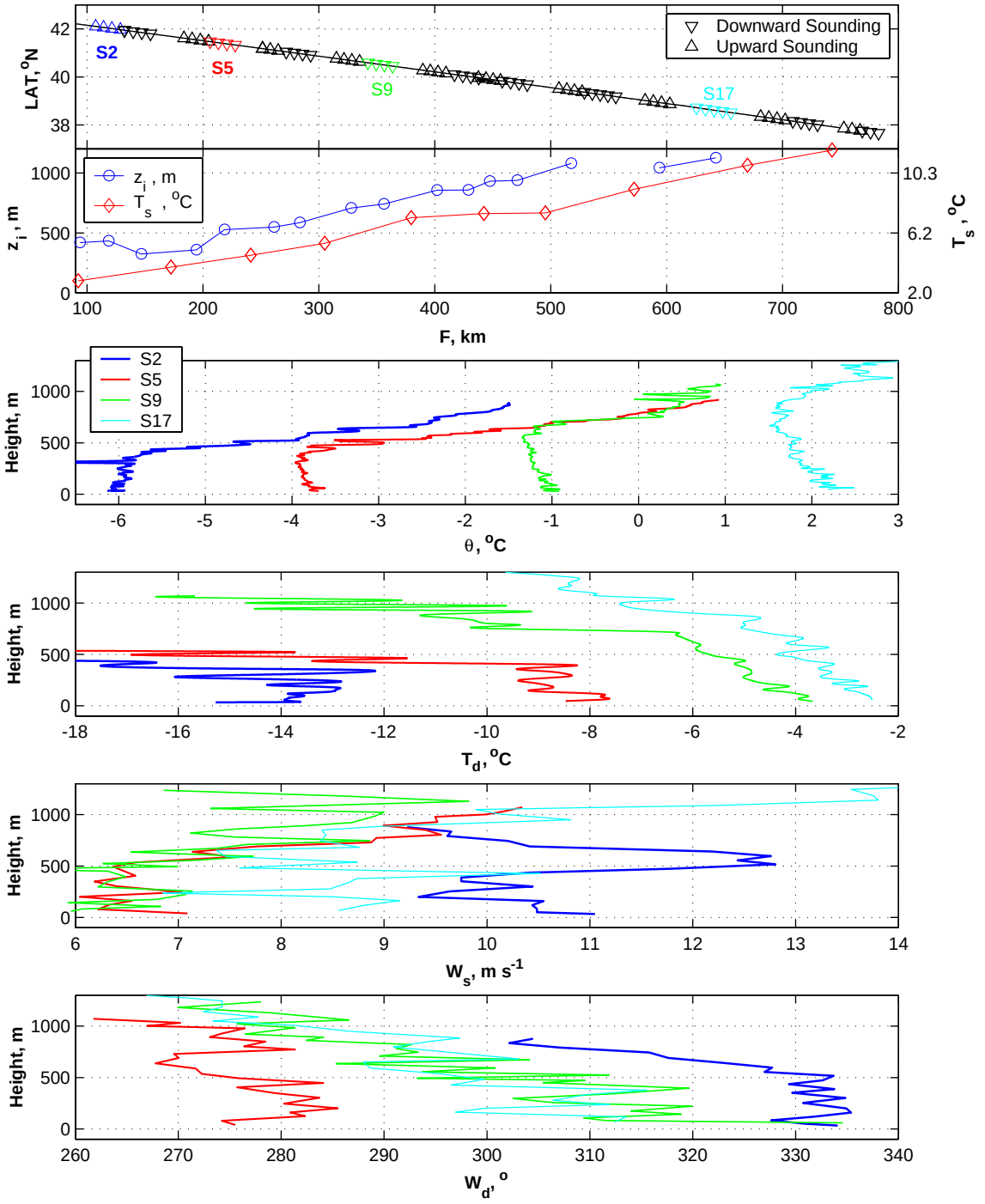

Fig. 7. Vertical structure of MABL and growth of IBL across the JES with offshore fetch, F, along an approximate streamline on 000203. From top to bottom, flight track with up and down sounding pairs; IBL height, z_i (left ordinate) and radiometric sea-skin temperature, T_s (right ordinate); profiles of potential temperature (less 273.15 K), θ; dew point temperature, T_d; wind speed, W_s; and wind direction, W_d. The profiles shown are from the four select soundings S2, S5, S9 and S17 identified on the track plot.

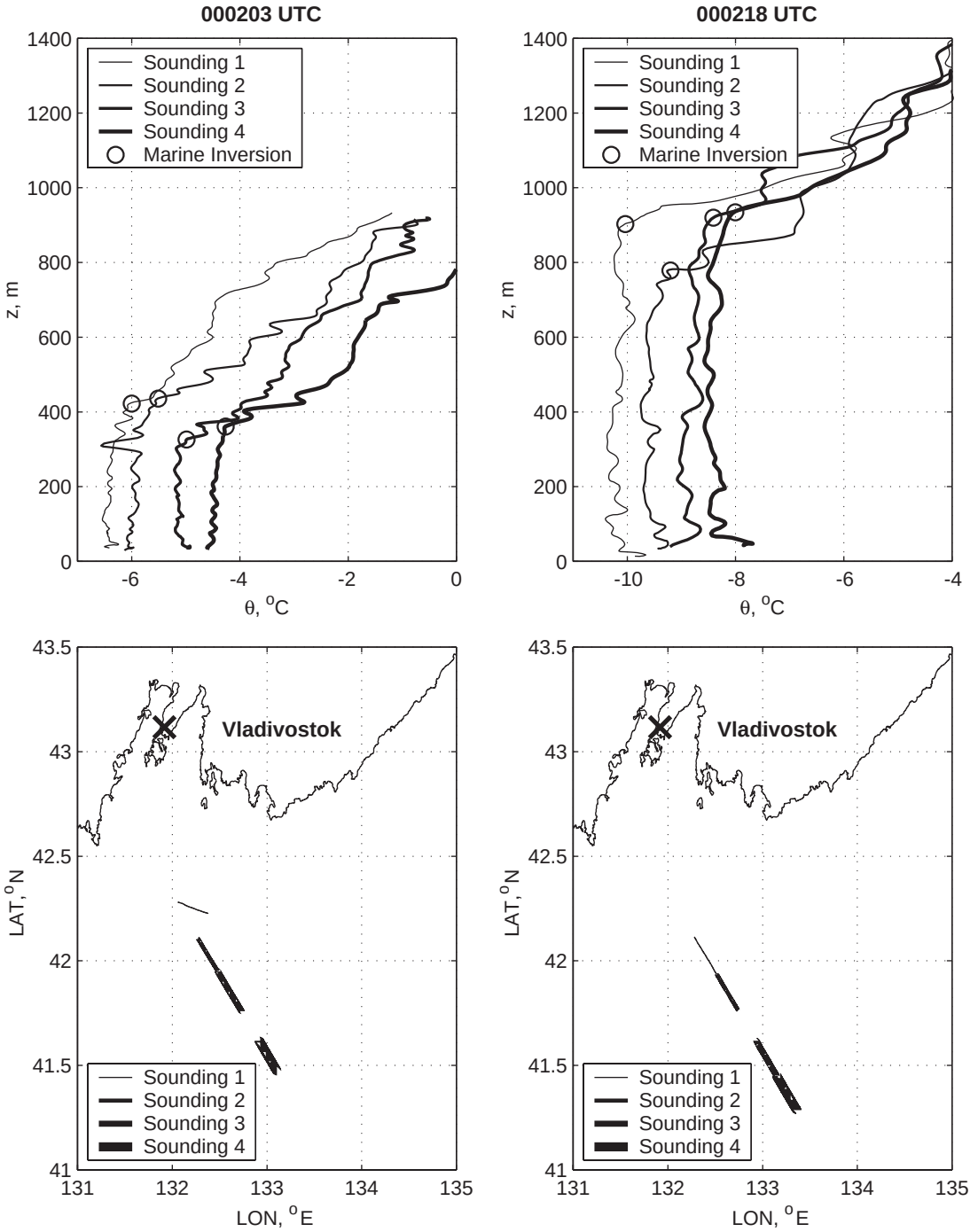

Fig. 8. Data from soundings nearest the Vladivostok gap from two IBL flights 000203 (left) and 00218 (right) showing potential temperature (less 273.15 K), θ, (top) and soundings tracks (bottom). Soundings 3 on 000203 and 2 on 000218, flown at almost the same location, show a thinning of the marine boundary layer. This may be due to the fanning out of the jet formed at the Vladivostok gap as it expands into the JES as suggested by the stratified flow model results of Scotti (2005). The IBL starts to grow afterwards as a result of the intense air–sea interaction.

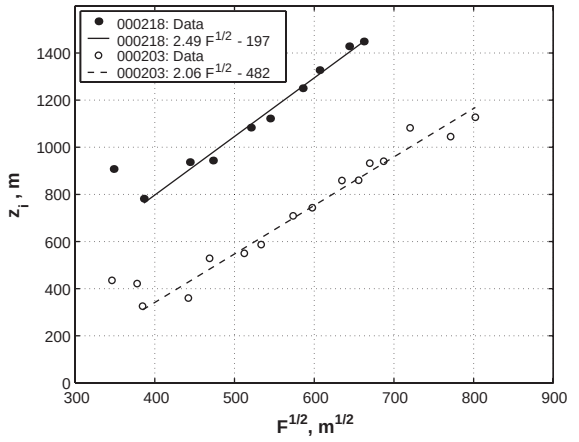

Fig. 9. IBL growth with square root of offshore fetch, F, and first-order least-square fits for an intense CAO day, 000218, and moderate CAO day, 000203 (symbols as indicated in figure).

data from a total of 73 low-level ($z<48$ m with a mean of 39.5 m) and straight runs flown in the Flux Center were averaged for each flight to yield ensemble averages of turbulent fluxes and surface meteorological variables on each mission day. It is hypothesized that these "daily" means are representative of the wintertime conditions in the Flux Center. The daily averages of Q_h, Q_e, τ, total turbulent heat loss from ocean, $Q_t=-(Q_h+Q_e)$, radiometric sea-skin temperature, T_s, ambient temperature, T_a, dew point temperature, T_d, barometric pressure, p, wind speed, W_s, and wind direction (meteorological convention), W_d, are shown in Fig. 10.

The sea-surface temperature measured by the radiometric pyrometer was found to exhibit large changes from just above 0 °C to 4 °C. This variability seems to be in response to the total surface heat flux as T_s and Q_t are positively correlated. Large sensible and latent-heat fluxes cooled the surface skin of the ocean. When $|Q_t|$ decreased, T_s increased. It is worth pointing out that T_s is the skin temperature inferred from the detected infrared radiation emanating from only the top 50 μm of the water and represents the true temperature of the air–sea interface (Katsaros, 1980). Also there appears to be a very close correlation between T_s and T_a where the two track each other resulting in an air–sea temperature difference approximately confined to the 7.5–10.8 °C range in the Flux Center. The stress is negatively correlated with T_s.

5.2. Comparisons with results of Kawamura and Wu (1998)

For the 12 aircraft flights, the measured surface fluxes in the Flux Center were in the ranges $\tau=0.01$–1.01 Pa, $Q_h=16$–231 W m^{-2}, and $Q_e=35$–187 W m^{-2}, with means of 0.348 Pa, 131 and 111 W m^{-2} and standard deviations of 0.21 Pa, 54 and 32 W m^{-2}, respectively. Compared to the minima of January 1997 means in the Flux Center of 0.275 Pa, 170 and 130 W m^{-2} determined by Kawamura and Wu (1998) for τ, Q_h and Q_e, respectively, the present findings are 27% higher for τ, 30% lower for Q_h and 17% lower for Q_e.

The reason for the discrepancies could be at least partly due to the relatively milder temperatures in the 0020131–000228 period of this study compared to the period 970101–970131 studied by Kawamura and Wu (1998). Measurements at the Vladivostok meteorological surface station showed that T_a varied mostly between −10 and −20 °C in the former study, whereas in this study it mostly fluctuated around −10 °C according to the findings of Dorman (2005). On the other hand, the mean W_s for this study was 13.4 m s^{-1}, whereas the maximum mean W_s from the contours in the Flux Center in Kawamura and Wu (1998) was only 10 m s^{-1} which may explain the larger τ found in this study. If the difference between the periods of the two studies was only in T_a, it would have resulted in much smaller Q_h and Q_e values. However, the larger W_s in this study would increase Q_h and Q_e but did not totally offset the effect of the net decrease in air–sea temperature difference between the two periods. It is worth noting that according to the data from the Vladivostok station reported by Dorman (2005), T_a also varied mainly between −10 and −20 °C in January 2000 just as it did in January 1997.

5.3. Variability across the JES

Although the main purpose of the IBL patterns was to provide sounding data, it was also possible to obtain 5 min of flux data at 30 m between two

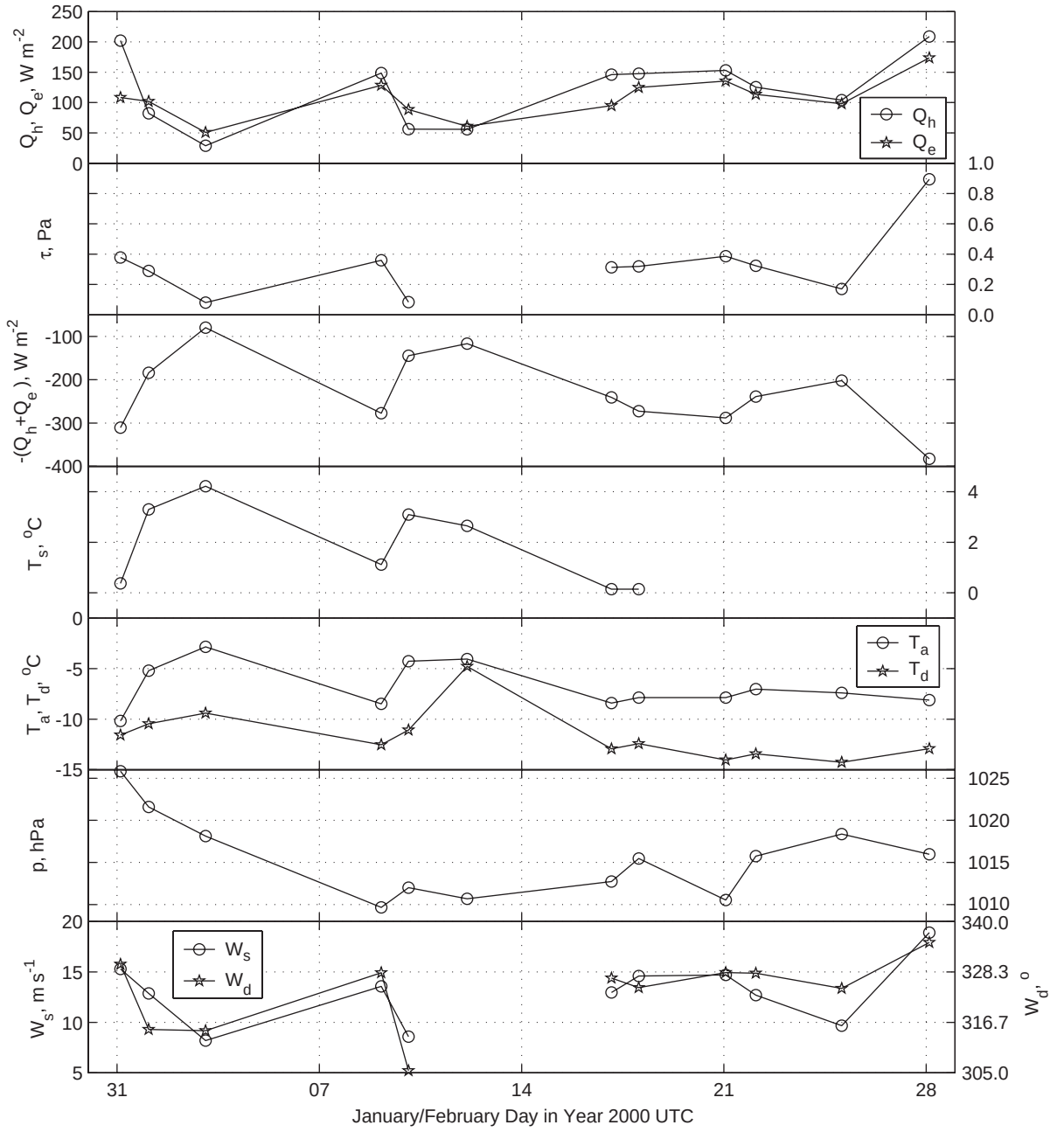

Fig. 10. "Daily" means of turbulent fluxes (determined from eddy correlation method using ogive technique) and meteorological data obtained from 73 level and straight runs below 48 m in the Flux Center. From top to bottom: sensible, Q_h, and latent, Q_e, heat fluxes; total stress τ; total turbulent heat loss from ocean, $-(Q_h + Q_e)$; radiometric sea-skin temperature, T_s; ambient temperature, T_a and dew point temperature, T_d; barometric pressure, p; and wind speed (left ordinate), W_s, and wind direction (right ordinate), W_d (meteorological convention).

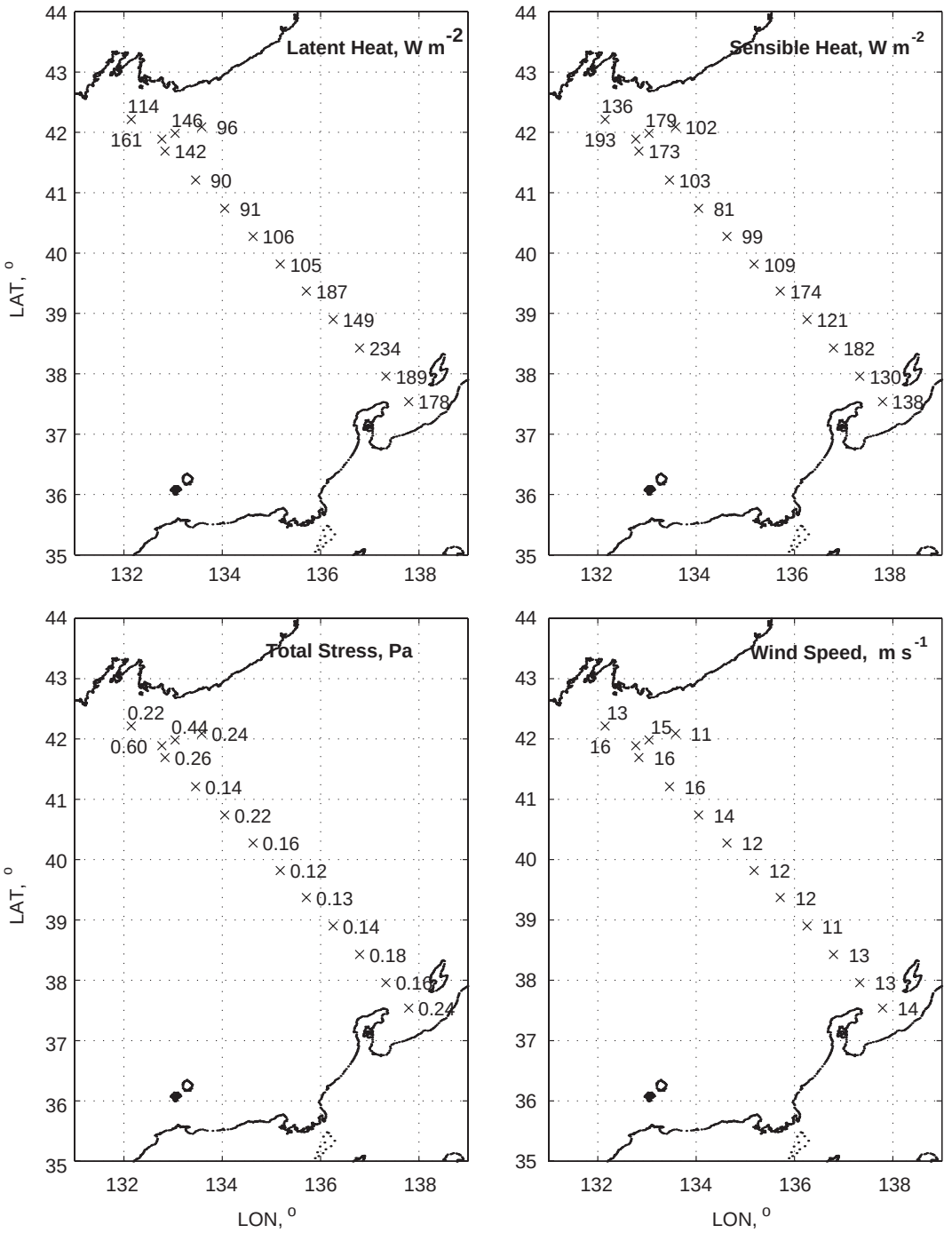

Fig. 11. Variability of turbulent fluxes across the JES on a cold-air outbreak (000218) during 01:20:50–04:04:05 UTC. The latent-heat (top, left), sensible-heat (top, right) and total stress (bottom, left) have large values in the Flux Center off Vladivostok. The heat fluxes are also high in the warmer SST region in southern JES. The wind speed (bottom, right) is given as an indication of the cold-air outbreak condition. The wind direction (not shown) backed from 340° in the North to about 300° mid-JES.

pairs of profiles. These are somewhat less reliable than those in the FM flights due to the shorter period. When an aircraft flies with or against the wind, longer run lengths or times are required compared to cross-wind runs due to the anisotropic nature of the flux-carrying eddies, especially the longitudinal roll vortices detected in the time series of Fig. 3 and the cospectra of Fig. 4. The 30-m IBL fluxes were estimated from the ogives; however, in some cases, estimates could not be determined. An example of the flux variability along an approximate streamline across the JES is shown in Fig. 11 for the CAO day on 000218. Large fluxes are observed south of Vladivostok in the Flux Center. A decrease is observed afterwards before both sensible and latent-heat fluxes increased at 39.5°N in response to the SST front and warmer surface waters in the southern JES and, possibly, due to orographic lifting nearest Honshu Island in the southernmost JES.

6. Bulk fluxes

Since the direct measurement of surface fluxes is only possible in a research setting, it is useful to examine the comparison of the directly measured fluxes with those estimated from the mean meteorological data using bulk aerodynamic formulas. The TOGA COARE algorithm (Fairall et al., 1996) was used, even though its calibration was for the tropical ocean. Comparisons of the sensible-heat, latent-heat and wind-stress fluxes obtained from the two methods are shown in Fig. 12 for a total of 114 combined (FM-IBL-FD) low-level ($z<48$ m with a mean of 39 m) flux runs. While there is the typical amount of scatter, the bulk vs eddy correlation averages for each flux over all results compare well: 0.291 vs 0.293 Pa, 130 vs 117 W m^{-2} and 122 vs 117 W m^{-2} with relative differences of −0.6%, 10.3% and 4.3% for τ, Q_h and Q_e, respectively. However, the comparison plots indicate that the bulk formulas underestimate the higher fluxes, especially for latent-heat and stress. The correlation as measured by the R-squared values between the bulk and direct measurement fluxes is relatively high for sensible-heat and momentum (0.70 and 0.67) but low for latent-heat (0.46).

The data from these comparisons were grouped by flight date and shown in Fig. 13. The largest discrepancies between the bulk and the eddy correlation estimates of Q_h and Q_e coincide with the period where the warmer radiometric sea-surface (which was used in the bulk calculations) was measured. The difference between the estimates of stress was largest on the last flight day 000228 when the highest winds and stresses were observed.

Bulk fluxes estimates also were calculated from simple bulk formulas using the constant transfer coefficients of $C_d = 1.27 \times 10^{-3}$ for τ and $C_h = C_e = 1.05 \times 10^{-3}$ for Q_h and Q_e which were determined as the median values of the transfer coefficients obtained from the (Fairall et al., 1996) algorithm run. The physical properties ρ, c_p and L_v used were calculated on each flux run from the mean values of the meteorological variables as in Section 3. When compared to the direct fluxes, the overall means of these bulk estimates were found the same for τ and Q_e, whereas Q_h was 18.5% higher. The R-squared correlation values were 0.68 for τ, 0.73 for Q_h and 0.48 for Q_e.

7. Model results

One of the goals of JES experiment was to provide detailed in situ measurements to be used for evaluation of mesoscale numerical models and to ultimately help improve their predictions. Because of the large horizontal and vertical boundary-layer coverage of research aircraft, the data obtained by the CIRPAS Twin Otter in JES are particularly suitable for comparison with models.

One such model is the three-dimensional non-hydrostatic Coupled Ocean/Atmosphere Mesoscale Prediction System (COAMPS) developed at the Naval Research Laboratory (NRL). Details of COAMPS can be found in Hodur (1997). The COAMPS simulations were started at 00 UTC on 000130 and continued through 000228. The model was initialized by the Naval Operational Global Atmospheric Prediction System (NOGAPS)

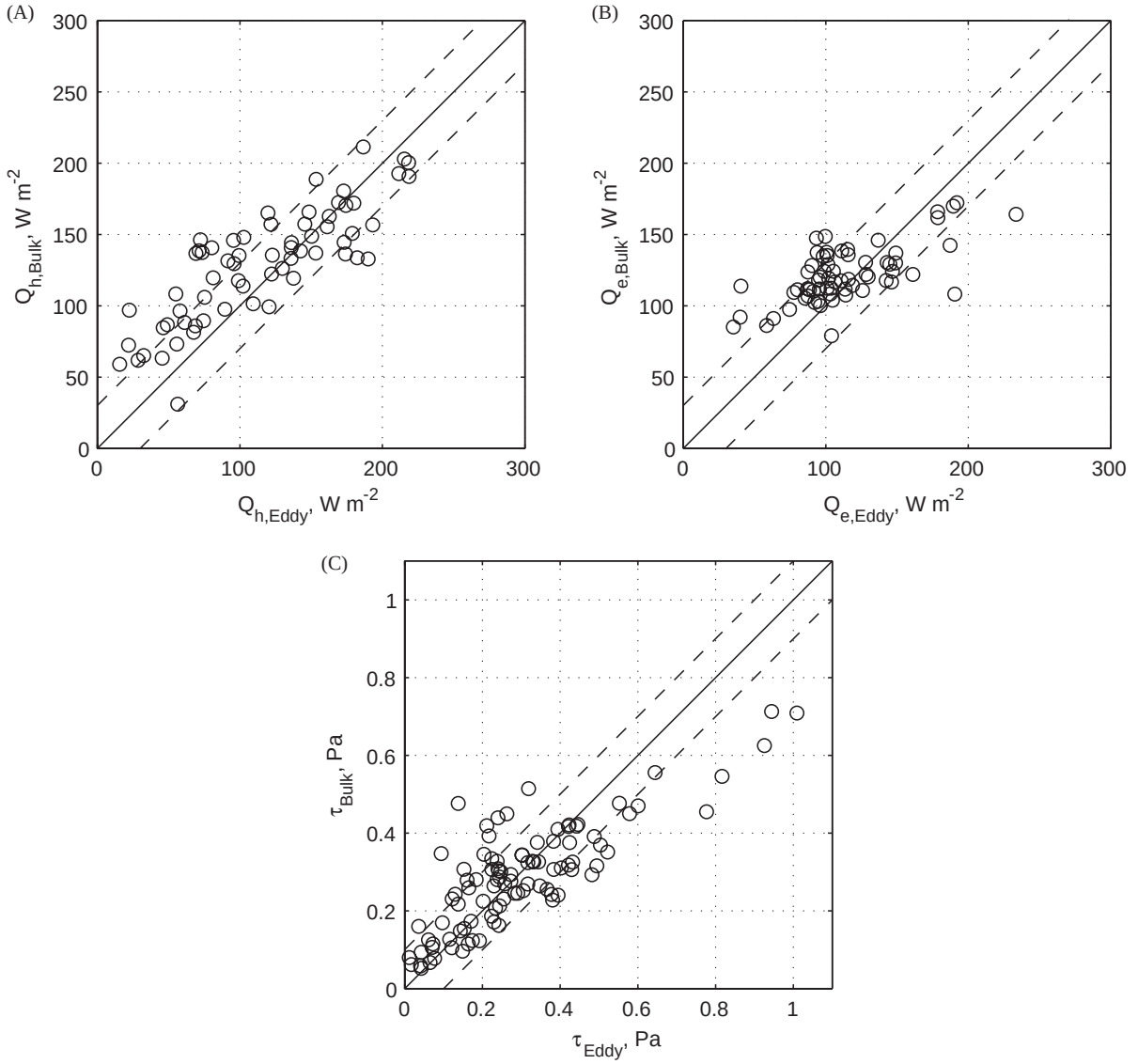

Fig. 12. Comparison of eddy correlation (abscissa) vs bulk (ordinate) fluxes of sensible-heat (A), latent-heat (B) and total stress (C). The TOGA COARE algorithm (Fairall et al., 1996) was used.

analysis field at the model starting time. The boundary conditions also came from NOGAPS analysis fields updated every 12 h. Three grid meshes were used with resolutions of 9, 27 and 81 km from the inner to the outermost nest, respectively, and 30 uneven levels in the vertical with about 10 levels within the atmospheric boundary layer. Data assimilation was made at 00 and 12 UTC each day for the outermost domain only to reduce the influence of the observations on the model results for the inner domain while keeping the inner domain boundary conditions as close as possible to the observed large-scale field. In the simulation, we used a Louis surface flux parameterization (Louis, 1979) modified to allow different roughness lengths for momentum and scalars. The Mellor–Yamada (Mellor and Yamada, 1982) level-2.5 boundary-layer scheme

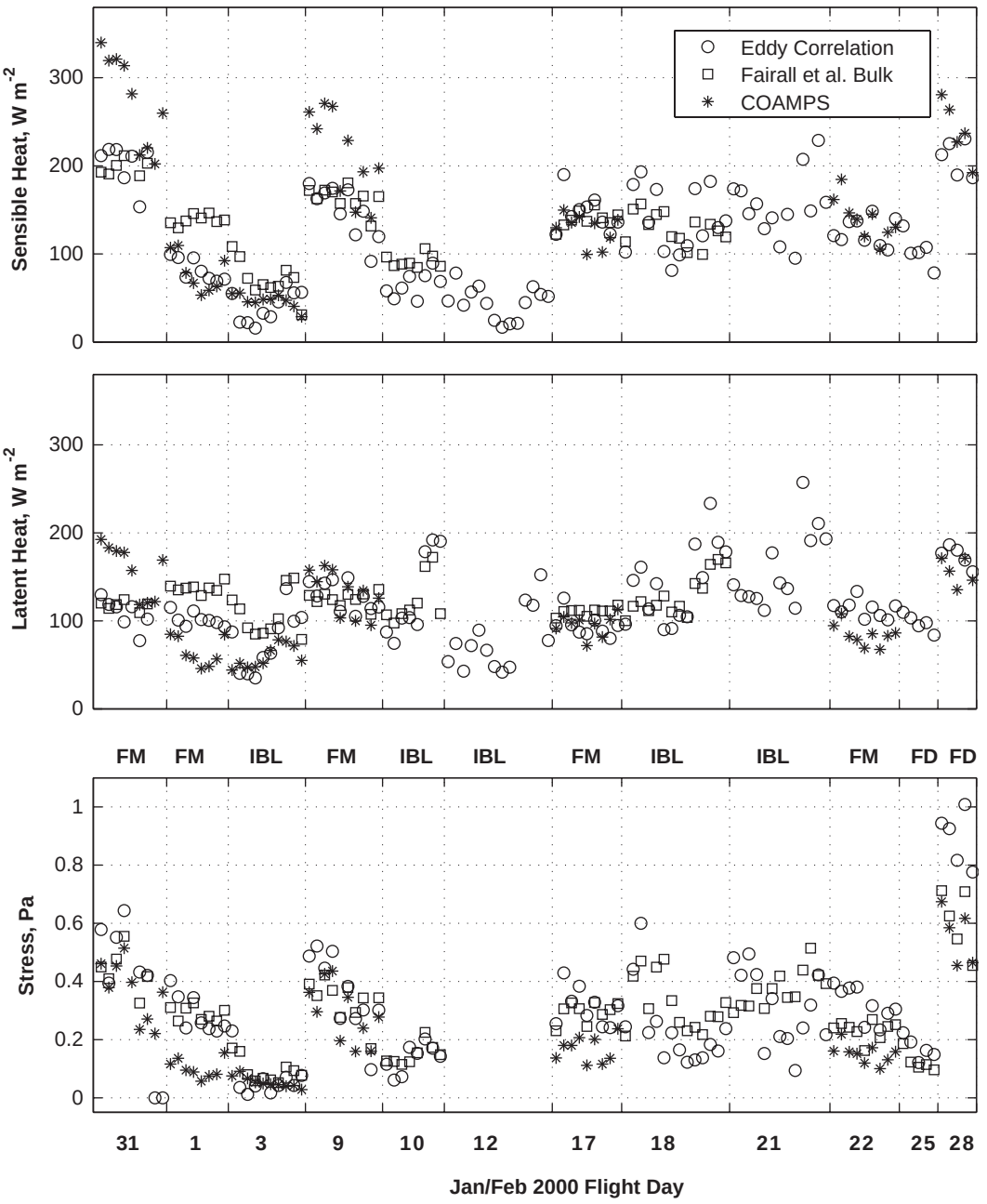

Fig. 13. Comparison of air–sea-surface sensible-heat flux (top), latent-heat flux (middle) and total stress (bottom) obtained from eddy correlation method, TOGA COARE bulk algorithm (Fairall et al., 1996) and COAMPS. (Symbols as indicated in figure.)

was used for boundary-layer turbulent mixing. The hourly results from COAMPS were taken as close as possible to the time and location of the aircraft observations.

Comparisons between aircraft covariance fluxes, Q_e, Q_h and τ, and mean meteorological variables, W_s, specific humidity, q, T_a and T_s and their counterparts predicted by COAMPS are shown in

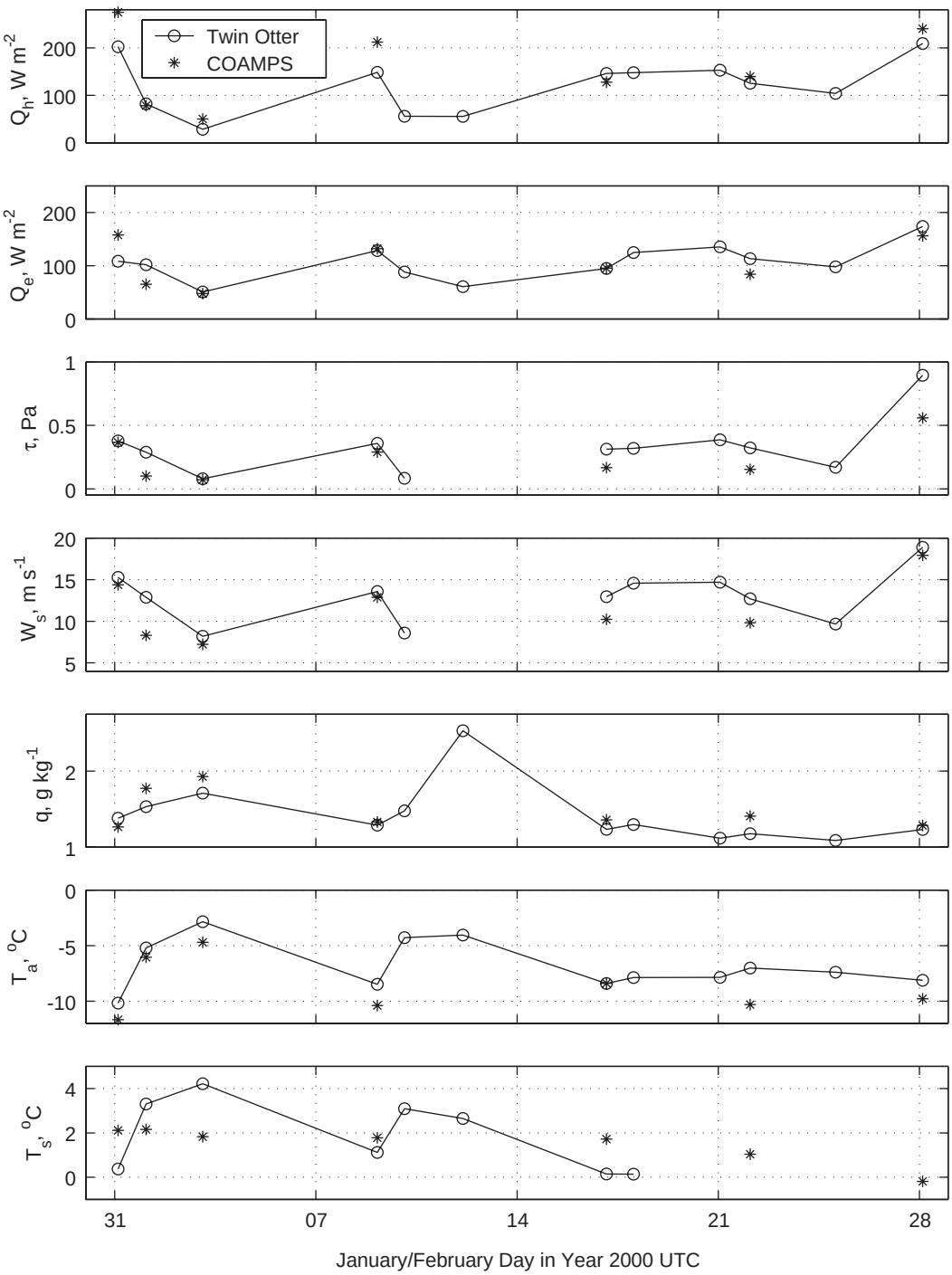

Fig. 14. Comparison between Twin Otter observations and COAMPS predictions of surface fluxes and mean meteorological variables. From top to bottom: sensible-heat, Q_h; latent-heat, Q_e; total stress, τ; wind speed, W_s; specific humidity, q; ambient temperature, T_a; and sea-surface temperature, T_s.

Fig. 14 as "Flux-Center-averages" (as described in Section 5.1). In general, the comparison is reasonable for the heat fluxes except for one or two days where differences were significant. COAMPS stress estimates were closer to the measured ones during the first half of the mission than during second part, where they were consistently smaller. The wind speed from COAMPS was also lower during that period except for the last day where it agreed with the 19 m s^{-1} value measured on that intense CAO day whereas the predicted stress was about 0.3 Pa less than the observed value. T_s from COAMPS remained unchanged at roughly 2 °C, whereas the radiometric T_s from the aircraft varied per discussion in Section 5.1. T_a results from COAMPS agreed about half of the time with the observations and were lower the other half. For the flight days where COAMPS results were available, the run-by-run flux comparisons with the eddy correlations fluxes are shown in Fig. 13 together with fluxes from (Fairall et al., 1996) bulk formulas. COAMPS predictions of Q_h seem to agree reasonably with the observations on 000201 when the rise in radiometric sea-skin temperature was observed and when the discrepancies between bulk and measured Q_h were the largest.

Fig. 15 shows COAMPS predictions of IBL heights and aircraft z_i data from the two IBL flights 000203 and 000218 discussed in Section 4. Although COAMPS seems to predict the growth of the IBL with offshore fetch, its IBL height values are much lower than those observed except for 000203 towards the start of the track in the Flux Center and at $F \approx 600$ km where they both indicate z_i values of about 325 and 1120 m for the two respective locations.

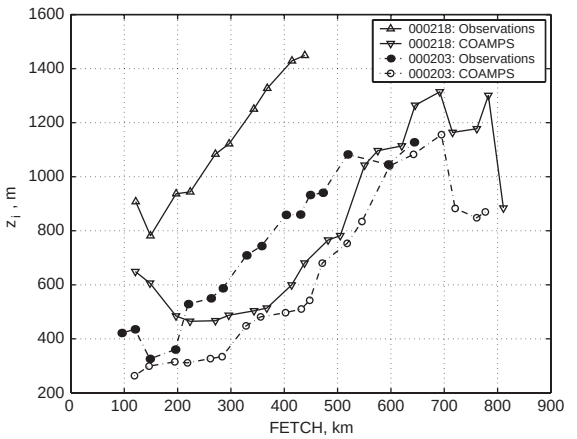

Fig. 15. Comparison of observed and COAMPS-predicted IBL height on an intense CAO day, 000218 and a mild CAO day, 000203 (symbols as indicated in figure).

8. Summary and conclusions

Detailed measurements of the boundary-layer structure and air–sea interaction over the wintertime JES were carried out with an instrumented aircraft in two basic flight patterns to study the internal boundary-layer (IBL) growth and surface flux mapping (FM) at approximately 30 m altitude.

The aircraft was able to explore the Flux Center region of the JES, as identified by Kawamura and Wu (1998). They defined the 1997 Flux Center as the area bounded by contours of 0.275 Pa for stress, 170 W m^{-2} for sensible-heat flux, and 130 W m^{-2} for latent-heat flux with maximum contours of 0.325 Pa, 210 W m^{-2} for stress and sensible-heat flux, respectively, and 400 W m^{-2} for combined latent and sensible-heat flux. The present aircraft results show high fluxes in the Flux Center, but no discernible spatial pattern. For the JES experimental period of late January–February 2000, the aircraft surface stresses were slightly larger than the threshold of Kawamura and Wu (1998), while the heat fluxes were slightly smaller. The aircraft-measured winds in the Flux Center were higher than the 1997 winds, as were the air temperatures. Apparently, the increased winds did not entirely compensate for the lower air–sea scalar differences and their combination resulted in lower heat fluxes than estimated by Kawamura and Wu (1998).

From the IBL transects across the JES, the surface fluxes generally decreased away from the Flux Center to minimums around the sea-surface temperature front near 40N, 135E, where the sensible and latent-heat fluxes increased thereafter to reach, near Honshu Island, values close to those in the Flux Center.

Surface fluxes directly calculated from the aircraft data were compared to the TOGA COARE

flux algorithm (Fairall et al., 1996) with reasonable correspondence. The calculated fluxes also agreed reasonably with estimates using constant coefficients $C_d = 1.27 \times 10^{-3}$ for τ and $C_h = C_e = 1.05 \times 10^{-3}$ for Q_h and Q_e. Correlation coefficients between the direct and bulk latent-heat fluxes, however, were not as high as for stress and sensible-heat.

The aircraft was equipped with an infrared radiometric thermometer that responds to the skin temperature of the ocean, T_s. The skin temperature in the Flux Center was found to vary considerably throughout the experimental period, ranging from slightly greater than 0 °C to 4 °C. The air and dew point temperatures tracked T_s. T_s was positively correlated with the total of the sensible and latent-heat flux loss from the ocean and negatively correlated with wind-stress. (See Fig. 10.)

The IBL inversion height was observed to grow linearly with the square root of offshore fetch in response to the total turbulent heat (latent + sensible) transfer from the ocean to the cold and dry continental air adverted across the JES. The spatial growth rates were $2.49\,m^{1/2}$ for an intense CAO day (000218) and $2.06\,m^{1/2}$ for a mild CAO (000203). Correlation R-squared values were high, 0.99 and 0.97, respectively.

Soundings from several flights nearest Vladivostok revealed an initial decrease in the inversion height, z_i, at 41.86°N, 132.6°E (Fig. 8). The initial thinning of the marine layer may be due to the jet flow out of the Vladivostok gap fanning out as it expands onto the open ocean. Results from the shallow-layer model of Scotti (2005) suggest the existence of such stratified flow dynamics.

The three-dimensional non-hydrostatic COAMPS model (Hodur, 1997) was run for the whole duration of the aircraft mission period. Reasonable agreement was in general found for the mean meteorological variables and the sensible and latent-heat fluxes. The model surface stresses were smaller for the second half of the comparison period. The sea-surface temperature from COAMPS was fairly constant at about 2 °C, whereas the radiometric T_s from the aircraft showed significant variability. The growth of the IBL with fetch was predicted by COAMPS, but the values of the IBL inversion height were much lower than those observed especially for the stronger cold-air outbreak day where the ratio between the two heights was in general less than half.

In conclusion, the aircraft measurements captured many of the features of cold-air outbreak conditions—the large surface fluxes, growth of the internal boundary layer, response of the surface temperature and downstream flux variation across the JES. Comparison to the COAMPS model is reasonable in some aspects. Further analysis of the flux divergence in the boundary layer, refinement of the bulk formula parameters will improve understanding of air–sea interaction and boundary-layer structure under these energetic conditions.

Acknowledgements

The experiment would not have been possible without the enthusiastic support of CIRPAS. We especially thank the chief pilot Mike Hubbell, co-pilot Jon Stairs, relief pilot Randy Goken for the long flights under harsh conditions and the support crew for their dedication. NAF Misawa was very accommodating, and the assistance of the METOC personnel is greatly appreciated. This work was supported by the Office of Naval Research (ONR) with D.K. and C.A.F under Grant N00014-99-1-0205 and Q.W. under Grant N00014-00-WR20156 and N00014-01-WR20242.

References

Burns, S.P., Khelif, D., Friehe, C., Williams, A., Hignett, P., Grant, A., Hacker, J., Rogers, D., Bradley, E., Weller, R., Cronin, M., Anderson, S., Fairall, C., Paulson, C., 1999. Comparisons of aircraft, ship, and buoy meteorological measurements from TOGA COARE. Journal of Geophysical Research 104, 30853–30883.

Dorman, C.E., 2005. Japan Sea meteorology: summer and winter. Deep Sea Research II, this issue.

Etling, D., Brown, R.A., 1993. Roll vortices in the planetary boundary layer: a review. Boundary-Layer Meteorology 65, 215–248.

Fairall, C.W., Bradley, E.F., Rogers, D.P., Edson, J.B., Young, G.S., 1996. Bulk parameterization of air–sea fluxes for Tropical Ocean-Global Atmosphere Coupled-Ocean Atmosphere Response Experiment. Journal of Geophysical Research 101, 3747–3764.

Friehe, C.A., Shaw, W.J., Rogers, D.P., Davidson, K.L., Large, W.G., Stage, S.A., Crescenti, G.H., Khalsa, S.J.S., Greenhut, G.K., Li, F., 1991. Air–sea fluxes and surface-layer turbulence around a sea-surface temperature front. Journal of Geophysical Research 96 (C5), 8593–8609.

Hartmann, J., Christoph, K., Siegfried, R., 1997. Roll vortices and boundary-layer development during a cold air outbreak. Boundary-Layer Meteorology 84, 45–65.

Hodur, R.M., 1997. The Naval Research Laboratory's Coupled Ocean/Atmosphere Mesoscale Prediction System (COAMPS). Monthly Weather Review 125, 1414–1430.

Hsu, A., 1986. Note on estimating the height of the convective internal boundary layer near shore. Boundary-Layer Meteorology 35, 311–316.

Katsaros, K.B., 1980. The aqueous thermal boundary layer. Boundary-Layer Meteorology 18, 107–127.

Kawamura, H., Wu, P., 1998. Formation mechanism of Japan sea proper water in the flux center off Vladivostok. Journal of Geophysical Research 103 (C10), 21611–21622.

Khelif, D., Burns, S.P., Friehe, C.A., 1999. Improved wind measurements on research aircraft. Journal of Atmospheric and Oceanic Technology 16 (7), 860–875.

Louis, J.F., 1979. A parametric model of vertical eddy fluxes in the atmosphere. Boundary-Layer Meteorology 17, 187–202.

Manabe, S., 1957. On the modification of air-mass over the Japan Sea when the outburst of cold air predominates. Journal of Meteorological Society Japan 35 (6), 311–326.

MEDOC Group, 1970. Observation of formation of deep water in the Mediterranean Sea, 1969. Nature 277, 1037–1040.

Mellor, G.L., Yamada, T., 1982. Development of a turbulence closure for geophysical fluid problems. Review of Geophysics and Space Physics 20, 851–875.

Renfrew, I.A., Moore, W.K., 1999. An extreme cold-air outbreak over the Labrador Sea: roll vortices and air–sea interaction. Monthly Weather Review 127, 2379–2394.

Scotti, A., 2005. Orographic effects during winter cold air outbreaks over the Sea of Japan (East Sea): results from a shallow layer model. Deep Sea Research II, this issue [doi:10.1016/j.dsr2.2004.06.038].

Stull, R.B., 1988. Boundary Layer Meteorology. Kluwer Academic Publishers, Dordrecht.

Venkatram, A., 1977. A model for internal boundary layer development. Boundary-Layer Meteorology 11, 419–437.